Article

Structural and Spectroscopic Characterization of Mononuclear Copper(I) Nitrosyl Complexes: End-on versus Side-on Coordination of NO to Copper(I)

Kiyoshi Fujisawa, Akira Tateda, Yoshitaro Miyashita, Ken-ichi Okamoto, Florian Paulat, V. K. K. Praneeth, Anna Merkle, and Nicolai Lehnert

J. Am. Chem. Soc., **2008**, 130 (4), 1205-1213 • DOI: 10.1021/ja075071d

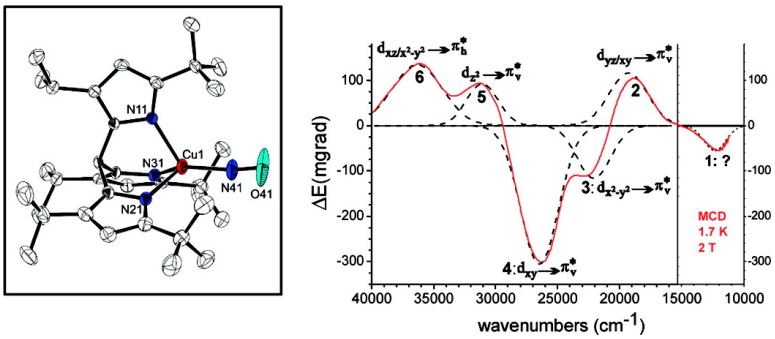

More About This Article

Additional resources and features associated with this article are available within the HTML version:

- Supporting Information
- Links to the 1 articles that cite this article, as of the time of this article download
- Access to high resolution figures
- Links to articles and content related to this article
- Copyright permission to reproduce figures and/or text from this article

View the Full Text HTML

J|A|C|S
ARTICLES
Published on Web 01/08/2008

Structural and Spectroscopic Characterization of Mononuclear Copper(I) Nitrosyl Complexes: End-on versus Side-on Coordination of NO to Copper(I)

Kiyoshi Fujisawa,*,† Akira Tateda,† Yoshitaro Miyashita,† Ken-ichi Okamoto,† Florian Paulat,‡ V. K. K. Praneeth,‡ Anna Merkle,‡ and Nicolai Lehnert*,‡

Graduate School of Pure and Applied Sciences, University of Tsukuba, Tsukuba 305-8571, Japan, and Department of Chemistry, University of Michigan, Ann Arbor, Michigan 48109

Received July 9, 2007; E-mail: kiyoshif@chem.tsukuba.ac.jp; lehnertn@umich.edu

Abstract: Two crystal structures of the mononuclear copper(I)−nitrosyl complexes [Cu(L3)(NO)] (**1**) and [Cu(L3′)(NO)](ClO_4) (**2**) with the related coligands L3$^-$ (hydrotris(3-*tert*-butyl-5-isopropyl-1-pyrazolyl)borate) and L3′ (tris(3-*tert*-butyl-5-isopropyl-1-pyrazolyl)methane) are presented. These compounds are then investigated in detail using a variety of spectroscopic methods. Vibrational spectra show ν(N−O) at 1698 cm^{-1} and ν(Cu−NO) split at 365/338 cm^{-1} for **1**, which translates to force constants of 12.53 (N−O) and 1.31 mdyn/Å (Cu−NO), respectively. The weak Cu−NO force constant is in agreement with the observed instability of the Cu−NO bond. Interestingly, complex **2** with the neutral coligand L3′ shows a stronger N−O bond, evident from ν(N−O) at 1742 cm^{-1}. This difference is attributed to a true second coordination sphere effect, where the covalency of the Cu(I)−NO bond is not altered. The EPR spectrum of **1** is in agreement with the Cu(I)−NO(radical) electronic structure of the complexes, as obtained from density functional theory (DFT) calculations. In addition, an interesting trend between $g_{\|}$(g_z) and the Cu−N−O angle is established. Finally, high-quality MCD spectra of **1** are presented and assigned using TD-DFT calculations. Based on the in-depth spectroscopic characterization of end-on bound NO to copper(I) presented in this work, it is possible to determine the binding mode of the Cu−NO intermediate of Cu nitrite reductase studied by Scholes and co-workers (Usov, O. M.; Sun, Y.; Grigoryants, V. M.; Shapleigh, J. P.; Scholes, C. P., *J. Am. Chem. Soc.* **2006**, *128*, 13102−13111) in solution as strongly bent (∼135°) but likely not side-on.

1. Introduction

The copper(I)−nitrosyl {CuNO}^{11} adduct[1,2] is a very important intermediate in the general reactions of copper proteins with biologically available nitrogen monoxide (commonly referred to as nitric oxide, NO).[3,4] For example, NO is believed to be a mediator of copper protein activity[5] and might also play a role in neurodegenerative diseases.[6] In particular, Cu nitrite reductase (CuNIR) is involved in the generation (and presumably degradation) of NO in denitrifying bacteria.[7,8] Crystal structures of a large number of CuNIR's have been determined, which show great similarities for the enzymes obtained from different organisms.[9] CuNIR's are homotrimers where each subunit contains one copper type 1 center for electron transfer. The catalytically active type 2 centers are located at the respective interfaces of two subunits of the enzyme. In oxidized CuNIR, the type 2 centers are tetrahedrally coordinated by three histidines and a water molecule, where two histidines are provided by one subunit, whereas the third one comes from the adjacent subunit.[10−15] The observed coordination mode of nitrite to the oxidized active site is asymmetric η^2-O,O corresponding to the formation of a copper(II)−nitrito intermediate.[11,13,16,17] This binding mode is also observed in a large number of

† University of Tsukuba.
‡ University of Michigan.

(1) In the Enemark−Feltham notation,[2] the number of d electrons of the metal plus the unpaired electron of NO are added up and then used as a superscript (here: 11). This allows for a classification of transition metal nitrosyls, in the case of which the assignment of metal and NO oxidation states is sometimes very difficult.

(2) Enemark, J. H.; Feltham, R. D. *Coord. Chem. Rev.* **1974**, *13*, 339−406.
(3) Shiva, S.; Wang, X.; Ringwood, L. A.; Xu, X.; Yuditskaya, S.; Annavajjhala, V.; Miyajima, H.; Hogg, N.; Harris, Z. L.; Gladwin, M. T. *Nat. Chem. Biol.* **2006**, *2*, 486−493.
(4) Bryan, N. S.; Fernandez, B. O.; Bauer, S. M.; Garcia-Saura, M. F.; Milsom, A. B.; Rassaf, T.; Maloney, R. E.; Bharti, A.; Rodriguez, J.; Feelisch, M. *Nat. Chem. Biol.* **2005**, *1*, 290−297.
(5) Torres, J.; Svinstunenko, D.; Karlsson, B.; Cooper, C. E.; Wilson, M. T. *J. Am. Chem. Soc.* **2002**, *124*, 963−967.
(6) Sorenson, J. R. J. *J. Inorg. Biochem.* **2001**, *87*, 125−127.
(7) Averill, B. A. *Chem. Rev.* **1996**, *96*, 2951−2964.
(8) Wasser, I. M.; de Vries, S.; Moënne-Loccoz, P.; Schröder, I.; Karlin, K. D., *Chem. Rev.* **2002**, *102*, 1201−1234.
(9) Suzuki, S.; Kataoka, K.; Yamaguchi, K. *Acc. Chem. Res.* **2000**, *33*, 728−738.
(10) Godden, J. W.; Turley, S.; Teller, D. C.; Adman, E. T.; Liu, M. Y.; Payne, W. J.; LeGall, J. *Science* **1991**, *253*, 438−442.
(11) Adaman, E. T.; Godden, J. W.; Turley, S., *J. Biol. Chem.* **1995**, *270*, 27458−27474.
(12) Murphy, M. E. P.; Turley, S.; Kukimoto, M.; Nishiyama, M.; Horinouchi, S.; Sasaki, H.; Tanokura, M.; Adman, E. T. *Biochemistry* **1995**, *34*, 12107−12117.
(13) Murphy, M. E. P.; Turley, S.; Adman, E. T. *J. Biol. Chem.* **1997**, *45*, 28455−28460.
(14) Dodd, F. E.; Van Beeumen, J.; Eady, R. R.; Hasnain, S. S. *J. Mol. Biol.* **1998**, *282*, 369−382.
(15) Inoue, T.; Gotowda, M.; Deligeer; Kataoka, M.; Yamaguchi, K.; Suzuki, S.; Watanabe, H.; Gohow, M.; Kai, Y. *J. Biochem.* **1998**, *124*, 876−879.

Scheme 1. Different Binding Modes of NO to Copper

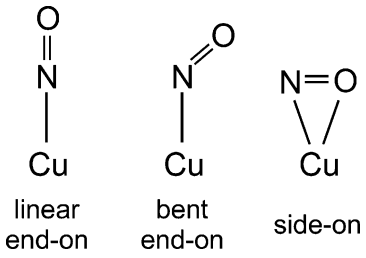

corresponding model complexes.[8,18] After completion of the catalytic cycle, NO (presumably coordinated to copper(II)) and water are generated. The exact mechanism for this conversion is still under discussion.[7,8,19] Interestingly, under anaerobic conditions with limited reductant and nitrite present, CuNIR is also able to act as an NO reductase by converting NO to N_2O,[20,21] a reaction that has also been observed for corresponding model complexes.[22] In this latter function, a $\{CuNO\}^{11}$ complex is most likely the catalytically active species.

In a recent study by Murphy and co-workers, a Cu(I)−NO intermediate of CuNIR, which was generated by exposing crystals of fully reduced CuNIR to NO saturated buffer, has been structurally characterized.[23] *Surprisingly, this species shows an unprecedented side-on coordination of nitric oxide to copper(I)* (cf. Scheme 1, right), which corresponds to a new intermediate in the biological chemistry of NO. Additional crystal structures that have just appeared in the literature confirm this result.[24] The authors also tried to generate this species in solution by treatment of ascorbate reduced CuNIR with NO under anaerobic conditions. From electron paramagnetic resonance (EPR) measurements on these solutions, the crystallograpically obtained $\{CuNO\}^{11}$ species was proposed to have a Cu(II)−NO^- electronic structure. These spectacular results, and in particular the unusual binding mode of nitric oxide to the copper(I) active site of CuNIR, have sparked interest in the coordination chemistry of copper(I) and NO and the spectroscopic properties of corresponding species.[25−27] Recently, Scholes and Solomon and co-workers have demonstrated spectroscopically that the solution species obtained by Murphy and co-workers is in fact a Cu(II)−NO_2^- complex.[21] Based on these results, these authors concluded that the crystallographically observed side-on $\{CuNO\}^{11}$ species is most likely not relevant for the catalytic cycle of the enzyme, because it is only generated in the crystal but not in solution in the presence of excess NO. In addition, density function theory (DFT) calculations clearly indicate that the side-on $\{CuNO\}^{11}$ intermediate should have a Cu(I)−NO(radical) electronic structure.[21,27] Independent of these studies, Scholes and co-workers have shown by EPR and electron−nuclear double resonance (ENDOR) spectroscopy that a $\{CuNO\}^{11}$ species can in fact be generated for CuNIR in solution by using fully reduced enzyme in the presence of limited amounts of NO.[26] From these studies, however, it is not clear whether the obtained $\{CuNO\}^{11}$ species shows end-on or side-on coordinated NO. Based on the crystal structure of a corresponding model complex (vide infra), some researchers favor the end-on binding mode of NO for this species.[21] On the other hand, the CuNIR crystal structure by Murphy and co-workers points toward a side-on coordination of NO.[23] The question of whether a side-on bound $\{CuNO\}^{11}$ species can exist is therefore of high significance for the understanding of the NO reductase activity of CuNIR but also of fundamental interest for the coordination chemistry of copper(I) and NO.

In light of this biological and medicinal significance of copper−nitrosyls, it is surprising that the biomimetic coordination chemistry of copper and NO and the investigation of the properties of these systems are not very developed. In fact, only one crystal structure of a mononuclear copper nitrosyl model complex has been reported so far by Tolman and co-workers, using $[HB(3\text{-}t\text{Bupz})_3]^-$ (Tp^{t-Bu}) as coligand.[28] Key spectroscopic data of this complex including the N−O stretch, EPR parameters, and electronic spectra were reported. Based on these data and unrestricted Hartree−Fock (UHF) calculations, the electronic structure of copper(I) NO complexes was described as Cu(I)−NO(radical). Besides this, a dinuclear copper−nitrosyl has been synthesized by Karlin and co-workers.[29]

In this work, two mononuclear copper nitrosyl complexes with anionic $[HB(3\text{-}t\text{Bu-}5\text{-}i\text{Prpz})_3]^-$ ($L3^-$)[18,30,31] and neutral $[HC(3\text{-}t\text{Bu-}5\text{-}i\text{Prpz})_3]$ (L3′)[31] coligands have been synthesized and structurally and spectroscopically characterized in detail. For this purpose, vibrational (IR), UV−vis absorption, EPR, and magnetic circular dichroism (MCD) spectroscopies have been applied. In correlation to DFT calculations, these data are analyzed in detail, and key insight about the nitrosyl binding to copper(I) is obtained. In addition, the effect of the total charge of the coligands on the properties of the Cu(I)−nitrosyls is discussed. Based on the detailed spectroscopic signature of end-on bound NO to copper(I) (cf. Scheme 1) elaborated here, the spectroscopic data obtained by Scholes and co-workers for the Cu(I)−NO complex of CuNIR in solution can be used to determine the binding mode of NO in this case. The conclusions drawn this way are further supported by DFT calculations.

2. Experimental Section

2.1. Materials. Preparation and handling of all complexes was performed under an argon atmosphere using standard Schlenk tube techniques or in an inert atmosphere glovebox. Anhydrous dichloromethane and chloroform were purchased from Aldrich Chemical Co. and stored in a glovebox. $^{15}N^{18}O$ gas was obtained from Shoko Co.,

(16) Strange, R. W.; Dodd, F. E.; Abraham, Z. H. L.; Grossmann, J. G.; Brüser, T.; Eady, R. R.; Smith, B. E.; Hasnain, S. S. *Nat. Struct. Biol.* **1995**, *2*, 287−292.
(17) Howes, B. D.; Abraham, Z. H. L.; Lowe, D. J.; Brüser, T.; Eady, R. R.; Smith, D. E. *Biochemistry* **1994**, *33*, 3171−3177.
(18) Lehnert, N.; Cornelissen, U.; Neese, F.; Ono, T.; Noguchi, Y.; Okamoto, K.; Fujisawa, K. *Inorg. Chem.* **2007**, *46*, 3916−3933.
(19) Kataoka, K.; Furusawa, H.; Takagi, K.; Yamaguchi, K.; Suzuki, S. *J. Biochem.* **2000**, *127*, 345−350.
(20) Casella, S.; Shapleigh, J. P.; Toffanin, A.; Basaglia, M. *Biochem. Soc. Trans.* **2006**, *34*, 130−132.
(21) Ghosh, S.; Dey, A.; Usov, O. M.; Sun, Y.; Grigoryants, V. M.; Scholes, C. P.; Solomon, E. I. *J. Am. Chem. Soc.* **2007**, *129*, 10310−10311.
(22) Ruggiero, C. E.; Carrier, S. M.; Tolman, W. B. *Angew. Chem., Int. Ed. Engl.* **1994**, *33*, 895−897.
(23) Tocheva, E. I.; Rosell, F. I.; Mauk, A. G.; Murphy, M. E. P. *Science* **2004**, *304*, 867−870.
(24) Tocheva, E. I.; Rosell, F. I.; Mauk, A. G.; Murphy, M. E. P. *Biochemistry* **2007**, *46*, 12366−12374.
(25) Antonyuk, S. V.; Strange, R. W.; Sawers, G.; Eady, R. R.; Hasnain, S. S. *Proc. Natl. Acad. Sci. U.S.A.* **2005**, *102*, 12041−12046.
(26) Usov, O. M.; Sun, Y.; Grigoryants, V. M.; Shapleigh, J. P.; Scholes, C. P. *J. Am. Chem. Soc.* **2006**, *128*, 13102−13111.
(27) Wasbotten, I. H.; Ghosh, A. *J. Am. Chem. Soc.* **2005**, *127*, 15384−15385.
(28) Ruggiero, C. E.; Carrier, S. M.; Antholine, W. E.; Whittaker, J. W.; Cramer, C. J.; Tolman, W. B. *J. Am. Chem. Soc.* **1993**, *115*, 11285−11298.
(29) Paul, P. P.; Tyeklar, Z.; Farooq, A.; Karlin, K. D.; Liu, S.; Zubieta, J. *J. Am. Chem. Soc.* **1990**, *112*, 2430−2432.
(30) Fujisawa, K.; Kobayashi, T.; Fujita, K.; Kitajima, N.; Moro-oka, Y.; Miyashita, Y.; Yamada, Y.; Okamoto, K. *Bull. Chem. Soc. Jpn.* **2000**, *73*, 1797−1804.
(31) Fujisawa, K.; Ono, T.; Ishikawa, Y.; Amir, N.; Miyashita, Y.; Okamoto, K.; Lehnert, N. *Inorg. Chem.* **2006**, *45*, 1698−1713.

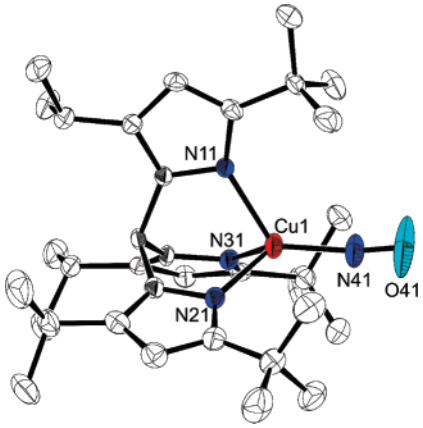

Figure 1. ORTEP view of [Cu(L3)(NO)] (**1**) showing 50% thermal ellipsoids and the atom labeling scheme. For clarity, hydrogen atoms were omitted. Selected bond distances (Å) and angles (deg): Cu1−N41 1.779(4), Cu1−N11 2.053(2), Cu1−N21 2.064(3), Cu1−N31 2.051(3), N41−O41 1.083(7), B1−N12 1.557(5), B1−N22 1.540(5), B1−N32 1.541(4); Cu1−N41−O41 171.9(5), N41−Cu1−N11 123.66(17), N41−Cu1−N21 122.81(18), N41−Cu1−N31 122.32(17), N11−Cu1−N21 91.85(12), N11−Cu1−N31 92.28(13), N21−Cu1−N31 95.61(14), N12−B1−N22 108.9(3), N12−B1−N32 109.8(3), N22−B1−N32 110.9(2).

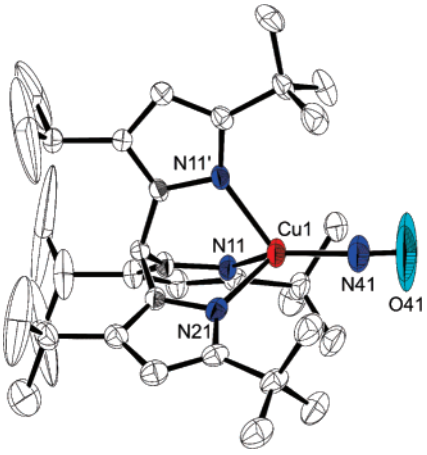

Figure 2. ORTEP view of the cation of [Cu(L3′)(NO)](ClO_4) (**2**) showing 50% thermal ellipsoids and the atom labeling scheme. For clarity, hydrogen atoms were omitted. Selected bond distances (Å) and angles (deg): Cu1−N41 1.786(5), Cu1−N11 2.070(3), Cu1−N21 2.058(4), N41−O41 1.035(8), C1−N12 1.451(4), C1−N22 1.448(7); Cu1−N41−O41 176.4(10), N41−Cu1−N11 125.09(14), N41−Cu1−N21 125.2(2), N11−Cu1−N21 90.68(12), N11−Cu1−N11′ 89.16(12), N12−C1−N22 112.2(2), N12−C1−N12′ 111.3(3). Symmetry code: $x, -y + {}^1/_2, z$.

Ltd and Aldrich Chemical Co. Other reagents are commercially available and were used without further purification. [Cu{HB(3-*t*Bu-5-*i*Prpz)$_3$}(NCMe)] ([Cu(L3)(NCMe)]) and [Cu{HC(3-*t*Bu-5-*i*Prpz)$_3$}-($OClO_3$)] ([Cu(L3′)($OClO_3$)]) were prepared according to published methods.[31] *Caution: Although we have not encountered any problems, it is noted that the perchlorate salts of metal complexes with organic ligands are potentially explosive and should be handled only in small quantities with appropriate precautions.* The elemental analyses (C, H, N) were performed by the Department of Chemistry at the University of Tsukuba.

2.2. Complex Syntheses. 2.2.1. [Cu(L3)(NO)] (1). [Cu(L3)-(NCMe)][31] (0.0616 g, 0.127 mmol) was dissolved in dichloromethane (2.0 mL) in a glovebox. The solution was cooled to −78 °C under an argon atmosphere, and argon was then replaced by NO. The solution was stirred for 1 h at −50 °C. The solution was kept at −30 °C for 1 day. The solution was then cooled down to −50 °C again. Crystallization from dichloromethane at −50 °C yielded red crystals (Figure 1). Elemental analysis (%) calcd for $C_{30}H_{52}N_7BCuO{\cdot}CH_2Cl_2$: C, 54.27; H, 7.93; N, 14.29. Found: C, 54.87; H, 8.14; N, 14.19. IR (KBr, cm^{-1}): 2965 ν(CH), 2564 ν(BH), 1698 $\nu(^{14}N^{16}O)$, [1627 $\nu(^{15}N^{18}O)$]. UV−vis λ/nm (ϵ/mol^{-1} dm^3 cm^{-1}) (dichloromethane), 506(960).

2.2.2. [Cu(L3′)(NO)](ClO$_4$) (2). [Cu(L3′)($OClO_3$)][31] (0.1290 g, 0.192 mmol) was dissolved in chloroform (8.0 mL) in a glovebox. The solution was cooled to −50 °C under an argon atmosphere, and argon was then replaced by NO. The solution was stirred for 1 h allowing the temperature to reach about −4 °C. The solution was further kept at −30 °C for 1 day. The solution was then cooled to −50 °C. Crystallization from chloroform at −50 °C yielded orange crystals (Figure 2). Elemental analysis (%) calcd for $C_{31}H_{52}N_7CuO_5Cl{\cdot}CHCl_3$: C, 46.81; H, 6.51; N, 11.94. Found: C, 47.18; H, 6.46; N, 11.48. IR (KBr, cm^{-1}): 2970 ν(CH), 1742 $\nu(^{14}N^{16}O)$, [1710/1666 $\nu(^{15}N^{18}O)$]. UV−vis λ/nm (ϵ/mol^{-1} dm^3 cm^{-1}) (chloroform), 458(1140).

Labeled nitrosyl complexes, [Cu(L3)($^{15}N^{18}O$)] and [Cu(L3′)($^{15}N^{18}O$)]-(ClO_4), were synthesized by using $^{15}N^{18}O$ in the same manner as described for complexes **1** and **2**, respectively.

We did not perform detailed decomposition kinetic measurements. The ν(N−O) peak of **2** had almost disappeared 15 h after MIR measurements in solid KBr disks (exposed to air for 15 h), whereas the corresponding band of **1** just became somewhat weaker (Figure S5). Therefore, the stability of **1** is clearly much larger than that of **2**.

2.3. Crystal Structure Determination. The detailed crystal data, data collection, and structural refinement parameters for **1** and **2** are given in Table S1. Complete atomic labels are shown in Figures S1 and S2. The diffraction data were measured on a Rigaku/MSC Mercury CCD system with graphite monochromated Mo Kα (λ = 0.710 69 Å) radiation at low temperature. All crystals were mounted on glass fiber using epoxy glue. The unit cell parameters of each crystal were obtained using Rigaku Daemon software and refined using CrystalClear on all observed reflections.[32] Data using 0.5° intervals in ϕ and ω for 35 s/frame (**1**) and for 30 s/frame (**2**) were collected with a maximum resolution of 0.77 Å (744 oscillation images). The highly redundant data sets were reduced using CrystalClear and corrected for Lorentz and polarization effects. An empirical absorption correction was applied for each complex.[33,34] Structures were solved by direct methods using the program *SIR*92.[35] The position of the metal atoms and their first coordination sphere were located from a direct method *E*-map; other non-hydrogen atoms were found in alternating difference Fourier syntheses[36] and least-squares refinement cycles. These were refined anisotropically during the final cycles (CrystalStructure).[33,34] Hydrogen atoms were placed in calculated positions. Higher *R* and GOF values are due to one disordered dichloromethane for **1** and disordered methyl carbons of the isopropyl groups of L3′ as well as disordered chloroform and perchlorate molecules for **2** in the unit cell. The O atoms (O41) and N atoms (N41) of the NO molecules in both structures show somewhat large thermal ellipsoids. This phenomenon has also been observed in Tolman's structure reported before.[28] This is probably due to the fact that, even at low temperature, the low-energy motions of NO (rotation, etc.) are not fully frozen, giving rise to thermal motion or slight disorder. Moreover, we observed these problems in Cu(I)−CO complexes even at low temperature.[31] Therefore, this is a common observation for Cu−X−O complexes with hydrotris(pyrazolyl)borate and tris(pyrazolyl)methane coligands. Crystallographic data and structure refinement parameters including the final discrepancies (R and R_w) are listed in Table S1. Crystallographic data have been deposited at

(32) Pflugrath, J. W. CrystalClear Ver. 1.3. *Acta Crystallogr.* **1999**, *D55*, 1718−1725.
(33) *CrystalStructure 3.70: Crystal Structure Analysis Package*, version 3.70; Rigaku and Rigaku/MSC: 2005.
(34) Watkin, D. J.; Prout, C. K.; Carruthers, J. R.; Betteridge, P. W. *Crystal Issue 10*; Chemical Crystallography Laboratory: Oxford, U.K., 1996.
(35) Altomare, A.; Cascarano, G.; Giacovazzo, C.; Guagliardi, A.; Burla, M.; Polidori, G.; Camalli, M. SIR 92. *J. Appl. Crystallogr.* **1994**, *27*, 435.
(36) Beurskens, P. T.; Admiraal, G.; Beurskens, G.; Bosman, W. P.; de Gelder, R.; Israel, R.; Smits, J. M. M. *The DIRDIF-99 program system*; Technical Report of the Crystallography Laboratory, University of Nijmegen: The Netherlands, 1999.

the CCDC, 12 Union Road, Cambridge CB2 1EZ, U.K., and copies can be obtained on request, free of charge, by quoting the publication citation and the deposition numbers: CCDC-615640 for **1** and CCDC-615641 for **2**.

2.4. Spectroscopic Measurements. UV−vis absorption data were recorded with an Otsuka Electronics MCPD-2000 system with an optical fiber attachment in the 300−1100 nm region at low temperature. The magnetic circular dichroism (MCD) setup consists of a JASCO J-810 spectropolarimeter and an Oxford Instruments SPECTROMAG SM4000 magnetocryostat. Samples for MCD were recorded in silicone oil (DC 200) mulls. EPR spectra were recorded on a Bruker EMX EPR spectrometer in frozen solution (CH_2Cl_2/$\{CH_2Cl\}_2$ (1:1)) in quartz tubes (diameter 5 mm) at 5−10 K with an Oxford Instruments liquid helium cryostat in the 2000−4200 G region. The spectrum of **1** shown in Figure 3 in red was measured at a frequency of 9.341 GHz and a microwave power of 20 mW. IR data were obtained with a JASCO FT/IR-550 spectrometer in the 4000−400 cm^{-1} region for MIR (middle-infrared) and 650−150 cm^{-1} for FIR (far-infrared) measurements.

2.5. Normal Coordinate Analysis. Normal coordinate calculations were performed using the QCPE computer program 576 by M.R. Peterson and D.F. McIntosh. The calculations are based on a general valence force field; force constants are refined with a nonlinear simplex algorithm. The simplex optimization was used to refine only *selected* force constants according to the quantum-chemical centered normal coordinate analysis (QCC-NCA) scheme.[37] Here, a force field from DFT calculations is used as a starting point to generate initial force constants, and a subset of these is fit to reproduce the known experimental frequencies. Force constants are extracted from the Gaussian output using a modified version of the program Redong (QCPE 628).[38]

For the QCC-NCA treatment, the BP86/TZVP optimized structure of model system [Cu(L0)(NO)] (see DFT part) has been used, but the Cu−N−O angle has been adjusted to 180° for simplification, which is very close to the experimentally determined value of 172°. The calculated force field for [Cu(L0)(NO)] (BP86/TZVP) has been applied. For the QCC-NCA, the Cu−NO and N−O force constants as well as the Cu−NO/N−O nondiagonal element have been fitted to reproduce the experimentally observed vibrational energies of the Cu−N−O unit. Importantly, the QCC-NCA treatment reproduces the split appearance of the Cu−NO stretch. In order to refine the vibrational energies of the two split components, the diagonal elements of the C−C−CH_3 bending coordinates of the pyrazolyl rings have been slightly adjusted (lowered by 0.04 mdyn/Å) compared to the DFT-predicted values. From these results, the Cu−NO stretch is mixed with a [Cu(L3)] skeletal bending mode, which is shown in Figure S8. This mode is predicted at 350 cm^{-1} in the calculations. The mixing between this core bending mode and ν(Cu−NO) is reproduced accurately in the QCC-NCA, which means that the [Cu(L3)] core modes are well described in the calculation. In the QCC-NCA fit, the component at lower energy has more Cu−NO character (from the potential energy distribution (PED)) and, correspondingly, a larger $^{15}N^{18}O$ isotope shift. Experimentally, this trend is reversed, as apparent from the inverse trend in the isotope shifts. The Cu−N−O bends are found in the 200−250 cm^{-1} region, with small isotope shifts of 2−4 cm^{-1}. They are strongly mixed with [Cu(L3)] skeletal modes.

2.6. Density Functional Theory (DFT) Calculations. The structures of the model complexes [Cu(L0)(NO)] (L0 = hydrotris(3,5-dimethyl-1-pyrazolyl)borate) and $[Cu(L0')(NO)]^+$ (L0′ = tris(3,5-dimethyl-1-pyrazolyl)methane) were fully optimized with BP86/TZVP using the program package Gaussian 03.[39] For these calculations, the TZVP basis set[40] has been applied as implemented in G03. For method calibration, the structures of these models have also been fully optimized using B3LYP/LanL2DZ, which applies Becke's three-parameter hybrid functional with the correlation functional of Lee, Yang, and Parr (B3LYP).[41−43] The LanL2DZ basis set consists of Dunning/Huzinaga full double-ζ (D95) basis functions[44] on first row and Los Alamos

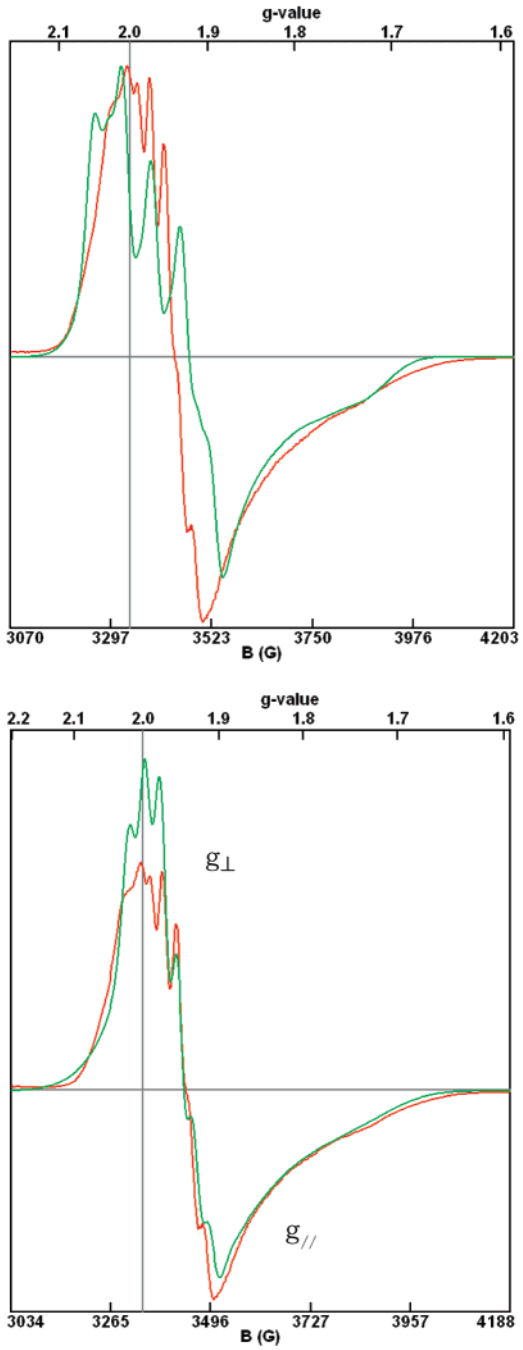

Figure 3. EPR spectrum of **1** at 5 K (red) including simulations (green). Top: for this simulation, the Cu hyperfine values determined by Tolman and co-workers (see ref 26 and 28) were used ($^{Cu}A_\perp$ = 187 MHz; $^{Cu}A_{||}$ = 320 MHz). However, the central region of the spectrum could not be fit this way. Bottom: alternative simulation, where the Cu hyperfine was allowed to vary stronger. Fit: g_x = 1.962, g_y = 1.972, g_z = 1.8; $^{Cu}A_x$ = 100 MHz, $^{Cu}A_y$ = 105 MHz, $^{Cu}A_z$ = 270 MHz; ^{14}N hyperfine (NO): $^{N}A_x$ = 98 MHz, $^{N}A_y$ = 19 MHz, $^{N}A_z$ = 17 MHz. Note that g_z could not exactly be determined due to lack of spectral resolution. The value of g_z is around 1.79−1.80.

(37) Praneeth, V. K. K.; Näther, C.; Peters, G.; Lehnert, N. *Inorg. Chem.* **2006**, *45*, 2795−2811.
(38) Allouche, A.; Pourcin, J. *Spectrochim. Acta* **1993**, *49A*, 571−580.
(39) Frisch, M. J. et al. *Gaussian 03*; Gaussian, Inc.: Pittsburgh, PA, 2003.
(40) Schäfer, A.; Horn, H.; Ahlrichs, R. *J. Chem. Phys.* **1992**, *97*, 2571−2577.
(41) Becke, A. D. *Phys. Rev. A* **1988**, *38*, 3098−3100.
(42) Becke, A. D. *J. Chem. Phys.* **1993**, *98*, 1372−1377.
(43) Becke, A. D. *J. Chem. Phys.* **1993**, *98*, 5648−5652.

effective core potentials plus DZ functions on all other atoms.[45,46] However, the obtained structures are in general inferior to the ones calculated with BP86/TZVP. In order to investigate whether B3LYP calculations can help improving the deviations in the Cu−N−O angle between the calculation and experiment, model [Cu(L0)(NO)] has also been fully optimized with B3LYP/TZVP and B3LYP/6-311G*. However, no improvement is observed as shown in Table S2. Calculated vibrational frequencies for all these geometry optimizations included in Table S2 show no imaginary modes, which shows that true energy minima have been obtained in all cases. Relative energies in Table 3 were either taken from BP86/TZVP calculations ("BP86") or from B3LYP/TZVP calculations ("B3LYP") on the BP86/TZVP optimized structures. EPR parameter (BP86/TZVP) and TD-DFT (B3LYP/TZVP) calculations were performed using the program package ORCA.[47] For Figure 4, the BP86/TZVP optimized structure of model [Cu(L0)(NO)] was used, and the Cu−N−O angle was adjusted correspondingly. For the geometry optimization of CuNIR models (cf. Figure 7), the crystal structure with bound NO (PDB:1SNR) from ref 23 was used together with the BP86/TZVP method. The histidines were fixed in space by freezing their anchor C atoms of the protein backbone, which where transformed into CH_3 groups for the calculations.

2.7. EPR Spectral Simulations. EPR spectra were simulated using the program SpinCount (version 2.2.40), written by Prof. Michael Hendrich, Carnegie Mellon University. EPR parameters are listed in the caption of Figure 3. The best fit is obtained with g_z around 1.79−1.80. The error bars for the hyperfine values are larger, around 5−10%.

3. Results and Analysis

3.1. Synthesis and Structural Characterization. The nitrosyl complexes [Cu(L3)(NO)] (**1**) and [Cu(L3′)(NO)](ClO_4) (**2**) were obtained from the reaction of [Cu(L3)(NCMe)] and [Cu(L3′)($OClO_3$)][31] with NO in good yield as shown in eq 1.

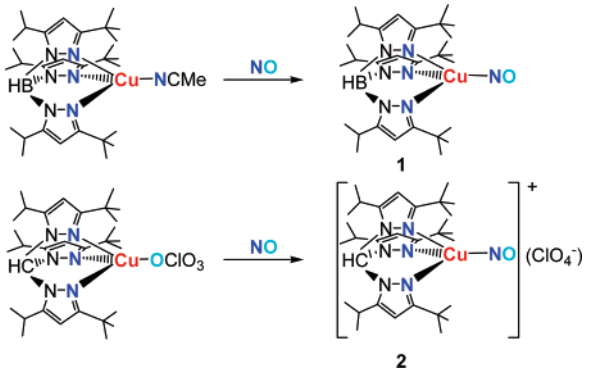

Detailed procedures are given in the Experimental Section. Complex **2** is very unstable toward NO loss (Figure S5). The structures of **1** and **2** determined by X-ray crystallography indicate that both complexes are mononuclear. As mentioned above, these compounds constitute only the second and third examples for mononuclear Cu(I)−NO model complex structures ever obtained in the literature. The perspective drawings of their structures are shown in Figures 1 and 2, respectively. In the copper nitrosyl complexes **1** and **2**, the copper ions have distorted tetrahedral coordination geometries. Cu−NO distances of **1** (1.779(4) Å) and **2** (1.786(5) Å) are similar and comparable to Tolman's compound [Cu(Tp^{t-Bu})(NO)] (**3**, 1.759(6) Å; cf. Table 1). On the other hand, the N−O distance of **1** (1.083(7) Å) is distinctively longer than that of **2** (1.035(8) Å), indicating potential differences in π backbonding (vide infra). Because of the difference in the total charge of the ligands ($L3^-$: anion, L3′: neutral), it is expected from previous work that π-backdonation in **1** is stronger than that in **2**,[31] which would be in agreement with the experimental trend. The copper ions are almost linearly ligated by NO in both cases (Cu−N−O angle = 171.9(5)° for **1** and 176.4(10)° for **2**). Although electronic effects usually predominate among the factors that induce nitrosyl bending,[28] the possibility that there are steric influences on the Cu−N−O angle is suggested by the observed orientation of the nitrosyl oxygen atom away from one of the *tert*-butyl groups and toward the open space between two pyrazolyl substituents in **3**. In this complex, the Cu−N−O angle is 163.4(6)°,[28] which is different from **1** and **2** reported here.

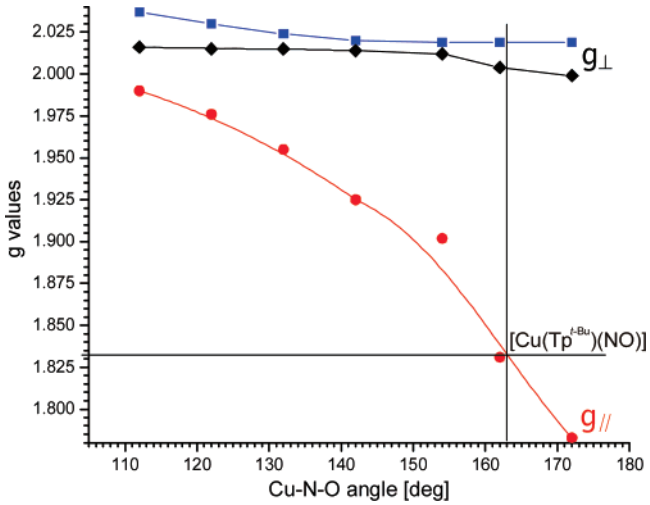

Figure 4. Calculated g values (BP86/TZVP) as a function of the Cu−N−O angle. Indicated are the predicted g values for **3**.

3.2. Vibrational Spectroscopy and Normal Coordinate Analysis. Tolman and co-workers reported the N−O stretching vibrations ν(N−O) for a number of [Cu(Tp)(NO)] type complexes (Tp^- = substituted hydrotris(pyrazolyl)borate),[28,48] but the critical Cu−NO stretch ν(Cu−NO) could not be identified. Clearly, the instability of the complexes renders the determination of high-quality vibrational data difficult. Figures S3 and S6 show the IR data of **1**, which show ν(N−O) at 1698 cm^{-1} and ν(Cu−NO) at 365 and 338 cm^{-1}. These bands shift to 1627, 358, and 332 cm^{-1} upon $^{15}N^{18}O$ substitution (cf. Table 1), respectively. To determine quantitative measures for the N−O and Cu−NO bond strengths and to explore the reason for the split appearance of ν(Cu−NO), a quantum-chemistry-centered normal-coordinate analysis (QCC-NCA)[37] was performed. As shown in Table 2, excellent agreement with experiment has been achieved, and the [Cu(L3)] skeletal mode that interacts with ν(Cu−NO) has been identified (see Figure S8). Obtained force constants are 12.53 (N−O) and 1.31 mdyn/Å (Cu−NO), where the latter value corresponds to a weak Cu−NO bond in agreement with the labile attachment of NO. In comparison, **2** exhibits ν(N−O) at 1742 cm^{-1}, and ν(Cu−NO) is tentatively assigned to the bands at 369 and 344 cm^{-1} (cf. Figures S4 and S7). Due to the poor quality of the far-infrared (FIR) data of

(44) Dunning, T. H., Jr.; Hay, P. J.; Schaefer, H. F., III. *Modern Theoretical Chemistry*; Plenum: New York, 1976.
(45) Hay, P. J.; Wadt, W. R. *J. Chem. Phys.* **1985**, *82*, 270−283 and 299−310.
(46) Wadt, W. R.; Hay, P. J. *J. Chem. Phys.* **1985**, *82*, 284−290.
(47) Neese, F. *ORCA*, version 2.2; Max-Planck Institut für Bioanorganische Chemie: Mülheim/Ruhr, Germany, 2004.
(48) Schneider, J. L.; Carrier, S. M.; Ruggiero, C. E.; Young, V. G., Jr.; Tolman, W. B. *J. Am. Chem. Soc.* **1998**, *120*, 11408−11418.

Table 1. Comparison of Experimental and Calculated Properties of Cu(I)−NO Complexes

	geometric parameters [Å]			vibrations [cm^{-1}]		force constants [b]	
complex	Cu–NO	N–O	Cu–N–O [a]	ν(N–O)	ν(Cu–NO)	f(N–O)	f(Cu–NO)
[Cu(Tp^{t-Bu})(NO)][c]	1.759(6)	1.108(7)	163.4(6)	1712			
[Cu(L3)(NO)]	1.779(4)	1.083(7)	171.9(5)	1698	365/(338)	12.53	1.31
[Cu(L3′)(NO)](ClO$_4$)	1.786(5)	1.035(8)	176.4(10)	1742	369/(344)		
Δ(L3′-L3)	**0.007**	**−0.048**	**4.5**	**44**	**4**		
			BP86/TZVP: full opt				
[Cu(L0)(NO)]	1.812	1.188	148	1707	456/(458)	12.72	2.22
[Cu(L0′)(NO)]$^+$	1.818	1.178	147	1758	453	13.56	2.14
Δ(L0′-L0)	**0.006**	**−0.010**	**−1**	**51**	**−3**	**0.84**	**−0.07**

[a] In degrees. [b] In [mdyn/Å]. [c] Reference 28.

Table 2. Comparison of Experimental and QCC-NCA Vibrational Frequencies [cm^{-1}] and of QCC-NCA and Calculated (DFT) Force Constants [mdyn/Å]

mode	exp.		QCC-NCA		Force constants f	
	n.a.i. [a]	$^{15}N^{18}O$	n.a.i. [a]	$^{15}N^{18}O$	QCC-NCA	Calculated [b]
[Cu(L3)(NO)] (**1**)						
ν(N-O)	1698	1627	1700	1625	12.530	12.72
ν(Cu-NO)[c]	365	358	366	363	1.310	2.22
	338	332	335	330		

[a] n.a.i = natural abundance isotopes. [b] Calculated with BP86/TZVP. [c] The Cu−NO stretch is mixed with a [Cu(L3)] core bending mode; see Experimental Section. Free NO: ν(N−O) = 1876 cm^{-1}; f_{N-O} = 15.49 mdyn/Å.[52]

this very labile complex, a QCC-NCA was not attempted. In previous studies of Cu(I)−carbonyl complexes, we determined that anionic "borate" type ligands like L3$^-$ lead to more electron-rich copper centers compared to analogous neutral "methane" ligands like L3′.[31] Hence, the borate complexes give rise to distinctively stronger π-backbonding interactions with CO, which is reflected by stronger Cu−CO and weaker C−O bonds. CO is therefore the perfect probe to measure the electronic properties of Cu(I).[31,48] *This trend is not followed by NO*: as evident from the vibrational data on **1** and **2**, and calculations on corresponding models as shown in Table 1, there is only a slight increase in the strength of the backbond in **1** compared to **2**. Correspondingly, the difference in (calculated) Cu−NO force constants is <0.1 mdyn/Å, and ν(Cu−NO) are similar. This small change in backbonding can only account for part of the observed large difference in the N−O bond strengths of **1** and **2**. The further weakening of the N−O bond in **1** is actually due to a stronger polarization of the π orbitals of NO and, hence, a true second coordination sphere effect in the case of **1**, due to the presence of the extra negative charge on the L3$^-$ ligand. This is evident from an inspection of the corresponding molecular orbitals from the DFT calculations (vide infra). Importantly, the calculations reproduce the difference in vibrational properties very well (compare Δ(L3′−L3) and Δ(L0′−L0) in Table 1). Interestingly, the experimental trend in ν(N−O) itself, [HB(3-CF$_3$-5-CH$_3$pz)$_3$]$^-$ ≥ L3′ > [HB(3,5-Ph$_2$pz)$_3$]$^-$ > [HB(3-*t*-Bupz)$_3$]$^-$ > L3$^-$, is similar to the trend observed for ν(C−O) in the carbonyl complexes.[31,48]

3.3. EPR Spectroscopy and Electronic Structure. Copper−nitrosyl {CuNO}^{11} adducts afford an $S = {}^1/_2$ ground state with characteristic EPR spectra: complex **3** exhibits $g_\perp = 1.99$ and $g_{||} = 1.83$ and a large ^{14}N hyperfine coupling $^{N}A_\perp = 81$ MHz as published by Tolman and co-workers.[28] In comparison, **1** shows $g_{||} = 1.79-1.80$, and $^{N}A_\perp = 98$ MHz as shown in Figure 3.[49] Comparison with the calculated g values in Table 3 reveals an interesting trend for the g values of Cu(I)−nitrosyls, where

Table 3. Calculated and Observed EPR Parameters of Cu(I)−NO Adducts

Complex	EPR parameters		Cu-N-O	ΔE [kcal/mol]	
	$g_\perp$	$g_{//}$	angle	BP86	B3LYP
Cu^I-NO in CuNIR [a]	2.046 1.998	1.926	?		
[Cu(Tp^{t-Bu})(NO)] [b]	1.99	1.83	163.4(6)		
[Cu(L3)(NO)]	~1.97	~1.80	171.9(5)		
[Cu(L0)(NO)] - calc.	2.019 2.012	1.902	154	0	0
[Cu(L0)(NO)] - 172° [c]	2.019 1.999	1.783	172	+0.8	+2.7
[Cu(L0')(NO)]$^+$ - calc.	2.015 2.012	1.907	155	0	0
[Cu(L0')(NO)]$^+$ - 174° [c]	2.016 1.998	1.786	174	+0.8	+0.7

[a] Reference 26. [b] Reference 28. [c] Obtained from the fully optimized structure (BP86/TZVP) by changing the Cu−N−O angle as indicated.

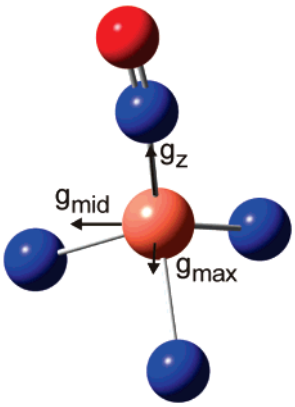

Figure 5. Calculated g tensor orientation for [Cu(L0)(NO)] with the Cu−N−O angle set to 172° (BP86/TZVP). In this case, g_z ($g_{||}$) equals g_{min} exactly, whereas g_{mid} and g_{max} approximately correspond to g_x and g_y in the coordinate system shown in Scheme 2, top. Note that g_z is collinear to the Cu−N bond.

$g_z = g_{||}$ (z points along the Cu−N(O) bond as indicated in Figure 5) is very sensitive to the Cu−N−O angle. In order to investigate this further, g values were calculated for model [Cu(L0)(NO)] varying the Cu−N−O angle, and these results are shown in Figure 4. Using the known Cu−N−O angle of 163° for **3**, $g_z = 1.833$ is predicted from Figure 4, which is in excellent agreement with the experimental value of 1.83 for this compound. In comparison, the Cu(I)−NO adduct of CuNIR shows very different g values as listed in Table 3,[26] indicative of a different coordination geometry (see Discussion). The obtained

(49) Unfortunately, we did not obtain good EPR data for **2**, due to decomposition.

Scheme 2[a]

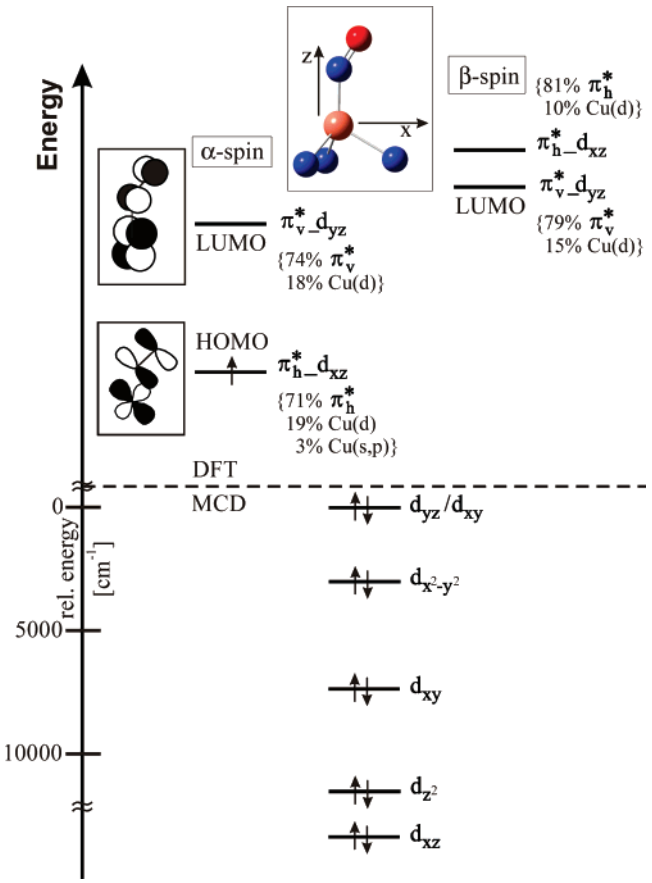

[a] Frontier orbitals of the fully optimized model [Cu(L0)(NO)] obtained from BP86/TZVP (upper part, spin unrestricted). The relative d-orbital energies are obtained from MCD (lower part, paired electrons).

hyperfine parameters $^{N}A_{\perp(x)} > 80$ MHz for **1** and **3** are very large and indicate *significant radical character on the bound NO ligand*. Scheme 2, top shows the binding scheme for **1** obtained from the DFT calculations. For the theoretical treatment, simplified model systems [Cu(L0)(NO)] and [Cu(L0′)(NO)](ClO$_4$) have been applied for **1** and **2**, respectively, as described in the Experimental Section. Different functional/basis set combinations have been used for the geometry optimizations as listed in Table S2. In general, good agreement with the experimental structures has been obtained, with exception of the Cu−N−O angle. In fact, none of the methods applied was able to reproduce the experimental value for this parameter. For further discussion, the BP86/TZVP results are used (cf. Tables 1−3). As indicated in Scheme 2, the singly occupied π^* orbital of NO ($\alpha-\pi^*_h$) is located in the Cu−N−O plane. Due to the fact that all copper(I) d orbitals are fully occupied, the overlap of this orbital with d_{xz} is actually repulsive for α-spin. This is compensated by the backbond between d_{xz} and the empty $\beta-\pi^*_h$ orbital. The strength of this interaction is best estimated from the corresponding antibonding combination, $\pi^*_h\_d_{xz}$, which has 10% metal d character. Altogether, this leads to a spin density distribution of +0.9 on NO and +0.1 on copper, in agreement with earlier calculations.[27] Hence, the calculations clearly favor the Cu(I)−NO(radical) over the Cu(II)−NO$^-$ electronic description in agreement with EPR and MCD (vide infra) results. The other π^* orbital, π^*_v (located perpendicular to the Cu−N−O plane), is unoccupied and undergoes further backbonding interactions. The corresponding antibonding combinations show about 15−20% d admixture, which corresponds to a quite strong interaction. However, comparison of the calculated Cu−NO force constant of 2.215 mdyn/Å with the experimental value of 1.310 mdyn/Å shows that the strength of this interaction is clearly overestimated in the calculations, which is not unusual.[37] The $\pi^*_v-d_{yz}$ backbond shows small spin-polarization effects (where the β-spin interaction is stronger), which somewhat lowers the total spin density on copper. This effect depends strongly on the applied DFT functional, which makes the prediction of very accurate total spin densities difficult. This bonding scheme is in agreement with the observed, large $^{N}A_{\perp(x)}$ value and also explains the observed strong dependence of g_z on the Cu−N−O angle (cf. Figure 4). This relates to the spin−orbit coupling matrix element $2\lambda\langle\pi^*_h\_d_{xz}|l_z|\pi^*_v\_d_{yz}\rangle/\Delta E$ in the theoretical equation for the g shifts from perturbation theory,[50]

$$g_i = g_e - 2\lambda \sum_{n\neq 0} \frac{\langle\Psi_0|L_i|\Psi_n\rangle\langle\Psi_n|L_i|\Psi_0\rangle}{E_n - E_0}$$

which maximizes at 180° when $\pi^*_h\_d_{xz}$ and $\pi^*_v\_d_{yz}$ become almost degenerate ($\Delta E \approx 0$).

3.3. Electronic Spectra. In previous work,[28] UV−vis absorption and MCD data above 300 nm have been presented for **3**, but no detailed analysis of the data has been provided. The characteristic absorption band at 494 nm for **3** has been loosely assigned to a Cu(I)-d to NO-π^* transition, but no further details are provided. As shown in Figure S9, this feature is observed at 506 nm ($\epsilon = 960$ M^{-1} cm^{-1}) for **1** and at 458 nm ($\epsilon = 1140$ M^{-1} cm^{-1}) for **2**. We have reinvestigated complex **1** using low-temperature MCD spectroscopy in silicone mulls, which allows for the measurement of high-quality data. Based on the spectrum obtained shown in Figure 6, five electronic transitions can actually be identified in the electronic spectra of the Cu(I)−NO complex (bands 2−6), and an additional weak feature is identified at 810 nm. These transitions can be assigned for the first time with the help of TD-DFT calculations. Application of B3LYP/TZVP and the experimental Cu−N−O angle of 172° reproduces the general shape of the electronic spectra well, but all transitions appear shifted to lower energy by ~4000 cm^{-1} (cf. Figure 6). This is due to the fact that all bands observed in the visible region correspond to CT transitions of type d → π^*, which are usually obtained too low in energy by TD-DFT. The tentative assignments as shown in Figure 6 are further supported by the appearance of pseudo-**A** term signals in the spectra (pairs of bands 2−3 and 4−5/6; see Table S3), which are in agreement with the calculated polarizations of these transitions. In order for a pseudo-**A** term to arise, two electronic transitions with orthogonal electric transition dipole moments are needed, which are coupled by spin−orbit coupling. These requirements are fulfilled by the given assignment (see Table S3). Based on these results, the medium strong absorption band of the Cu(I)−NO complexes in the visible region around 500 nm is due to d → π^*_v type CT transitions into the unoccupied π^*_v orbital of NO (bands 2−5, cf. Figure 6). The observed transition energies allow for the determination of the relative energies of the corresponding four d orbitals of highest energy, as included in Scheme 2,

(50) Lever, A. B. P.; Solomon, E. I. Ligand Field Theory and the Properties of Transition Metal Complexes. In *Inorganic Electronic Structure and Spectroscopy*; Solomon, E. I., Lever, A. B. P., Eds.; Wiley: New York, 1999; Vol. 1.

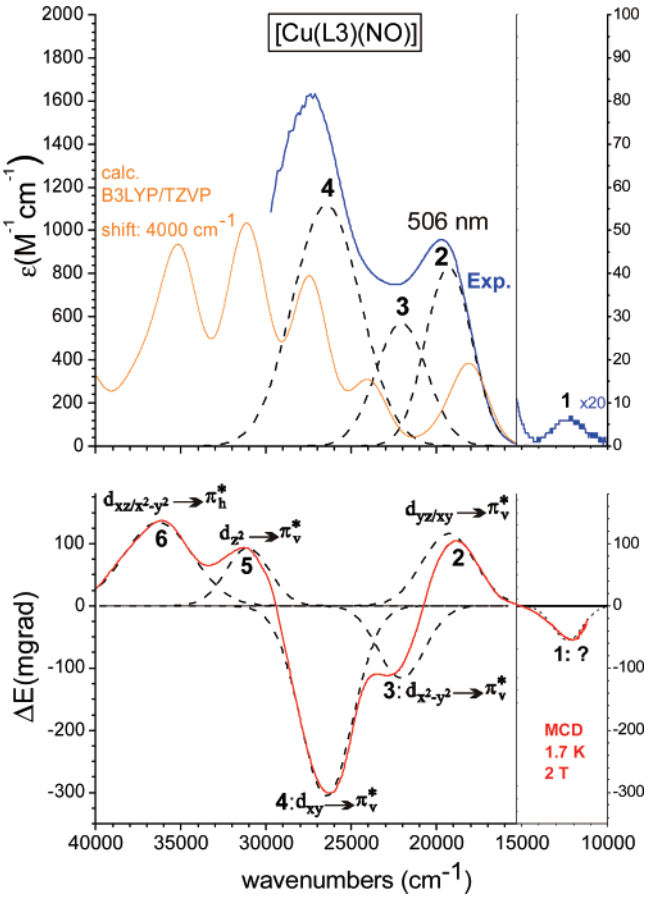

Figure 6. UV−vis (top) and MCD spectra (bottom) of **1** including Gaussians obtained from a correlated fit and TD-DFT based assignments. The TD-DFT calculated spectrum is shown in orange (shifted by 4000 cm^{-1} to lower energy in this figure).

bottom. The fifth d orbital, d_{xz}, is probably located at lowest energy in these complexes, due to a strong interaction with the singly occupied π^*_h orbital of NO. Since the corresponding CT transition is of d → π^*_h type (band 6, cf. Figure 6), the relative energy of this orbital cannot exactly be scaled to the other four d-orbitals as indicated in Scheme 2. Importantly, *the lack of intense (low-energy) d−d bands in the MCD spectra of* ***1*** *is a further indication that copper has a* d^{10} *electron configuration, in agreement with the Cu(I)−NO(radical) description of the end-on coordinated* {*CuNO*}^{11} *complexes* elaborated above. This is further supported by the TD-DFT results. Note that band 1 in Figure 6 corresponds to an impurity of [Cu^{II}(L3)(ONO)], which shows a very intense MCD transition in this area.[18] The observation of a very small amount of Cu(II) impurity is in agreement with corresponding, very weak features in the EPR spectra that account for about 5% of the total copper concentration.

4. Discussion

In this paper, two new crystal structures of mononuclear end-on Cu(I)−NO complexes are presented, and the first detailed spectroscopic analyses (vibrational and electronic) of this type of complexes are provided. Experimental force constants for [Cu(L3)(NO)] are 12.53 mdyn/Å (N−O) and 1.31 mdyn/Å (Cu−NO); the latter value is in agreement with the very labile Cu−NO bond in these systems. In comparison, the corresponding complex with a tris(pyrazolyl)methane ligand has a stronger N−O bond due to a second coordination sphere effect. The EPR spectrum of [Cu(L3)(NO)] is indicative of the Cu(I)−NO(radical) electronic structure of the complexes in agreement with the DFT results. Interestingly, the g_z value correlates very well with the geometric structure of the Cu−N−O unit and decreases upon increase of the Cu−N−O angle. Finally, high-quality MCD spectra of [Cu(L3)(NO)] are presented and assigned using TD-DFT calculations. These results provide the first in-depth assignment of the electronic spectra of the end-on {CuNO}^{11} species. In particular, the observed CT absorption band in the visible region is due to d → π^*_v type transitions. Based on the MCD results, an approximate determination of the d-orbital energy scheme for [Cu(L3)(NO)] is possible. Importantly, the lack of intense low-energy d−d bands in the MCD spectra is a further indication that copper has a d^{10} electron configuration, in agreement with the Cu(I)−NO(radical) description of the complexes.

In summary, based on the experimentally calibrated electronic structure description of end-on Cu(I)−NO complexes elaborated here, and in agreement with results published previously,[27,28] it is therefore now demonstrated that the Cu(I)−NO unit has to be described as Cu(I)−NO(radical).

The detailed spectroscopic characterization of end-on bound Cu(I)−NO complexes provided in this work allows us to draw further conclusions about the Cu(I)−NO intermediate observed by Scholes and co-workers for CuNIR in solution.[26] From their EPR and ENDOR results, it is not clear whether this species has end-on or side-on coordinated NO. Although the crystal structure of Murphy and co-workers shows side-on bound NO,[23] others have speculated that this structure is an "artifact" observed in the crystal but that this binding mode does not exist in solution. This opinion is supported by recent DFT calculations on the CuNIR active site, which predict that the end-on geometry is more stable by about 7 kcal/mol compared to the side-on bound species.[21] These contradictory findings pose the important question whether the side-on coordination mode of NO to Cu(I) is feasible or not. As we have demonstrated in this paper, the EPR g_z value of the Cu(I)−NO species shows a strong correlation with the Cu−N−O angle. Hence, *our EPR results in comparison with the data obtained by Scholes and co-workers for the Cu(I)−NO complex of CuNIR (cf. Figure 4) do in fact support a strongly bent or even side-on coordination of NO in the enzyme*. As shown in Table 3, the end-on bound Cu(I)−NO model complexes show g_z around 1.83, whereas, in the case of CuNIR, g_z is found at 1.93. Based on this, we believe that the Cu(I)−NO intermediate of CuNIR generated in the presence of low concentrations of NO does in fact show a strongly bent to side-on binding mode of NO. How is it possible, though, that the enzyme behaves so differently than the model complexes studied so far? A first indication as to why this is in fact possible comes from recent DFT results of Wasbotten et al.,[27] which show that the type of coligand bound to copper actually has a large influence on the relative energies of the end-on and side-on coordinated species. In order to further investigate this point, we have performed DFT geometry optimizations on the CuNIR active site with bound NO, where the three histidines are held in position by fixing their anchor C atoms (of the CH_3 groups) in space. For these calculations, the BP86/TZVP method has been applied again, which produces reasonable structures for the model complexes. As shown in Figure 7, the obtained Cu(I)−NO geometry from this calculation shows a Cu−N−O

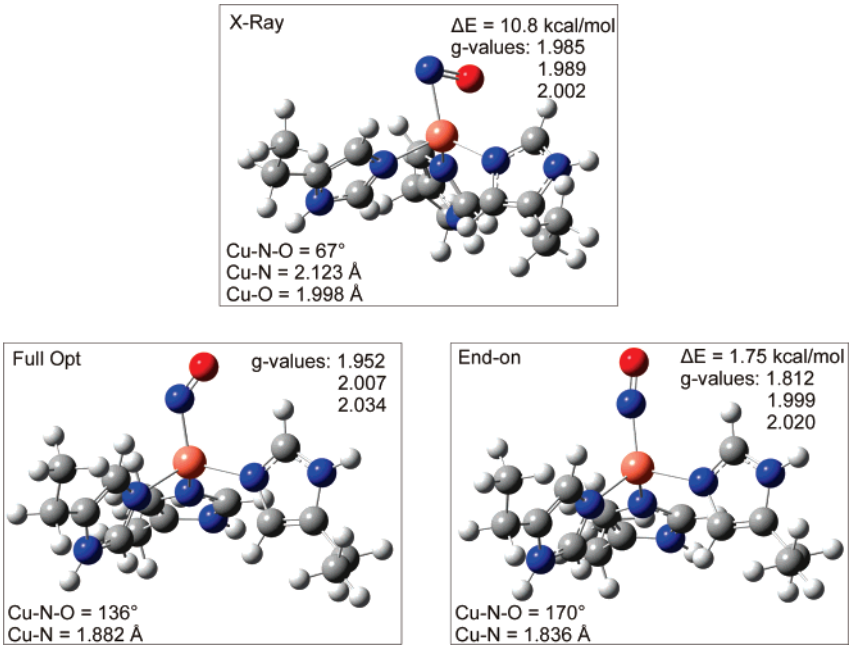

Figure 7. Geometry optimized (BP86/TZVP) structures of Cu(I)−NO species in CuNIR. For these calculations, the anchor atoms (C atoms of the artificial CH_3 groups) of the three histidines were frozen at their crystallographic positions. Top: optimized structure with frozen Cu−N−O angle at the crystallographically determined value.[23] Bottom, left: fully optimized structure. Bottom, right: optimized structure with frozen Cu−N−O angle at a value typical for the model complexes. Listed are relative energies with respect to the fully optimized structure and calculated *g* values for the three structures (BP86/TZVP).

angle of 136° (cf. Figure 7, bottom left), which is intermediate between end-on (>160°; from the model complexes) and side-on (71°; from Murphy's structure). We have further generated end-on and side-on bound structures for CuNIR by fixing the Cu−N−O angle at 170° and 67°, respectively, and reoptimization of the structures. The resulting geometries are shown in Figure 7 top and bottom right. To test whether these three structures also follow the trend in g_z values as described above, we have then calculated the *g* tensors for the three binding modes. Importantly, as shown in Figure 7, *the general trend in g values is in fact followed by the CuNIR models*. Based on these results, two important conclusions can be drawn:

(a) a strongly bent (and potentially side-on) coordination of NO to copper(I) is reasonable and depends on the coligand(s) bound to copper;

(b) the EPR parameters of the Cu(I)−NO species of CuNIR as determined by Scholes and co-workers[26] do in fact reflect a strongly bent or side-on coordination of NO to copper(I).

Comparison of the calculated *g* tensors with the *g* values obtained by Scholes and co-workers shows the best agreement between the fully optimized structure (Cu−N−O angle = 136°; cf. Figure 7, bottom left) and the experimental data. However, the calculated difference in *g* values between this structure and the side-on bound species is relatively small, so it would be unjustified to claim that the fully optimized structure exactly reflects the Cu(I)−NO geometry present in the enzymatic species detected in solution. Nevertheless, *the results clearly indicate that the Cu(I)−N−O unit is strongly bent in the enzyme in solution and not linear like in the model complexes.*

In summary, the geometry of the Cu(I)−NO subunit in proteins and model complexes has a much larger flexibility in terms of the coordination mode of NO and the Cu−N−O angle than previously anticipated from model complex studies. These results are also in agreement with the crystal structure of NO bound amine oxidase, which shows a Cu(I)−N−O angle of 117° (assuming that this species corresponds to a Cu(I)−NO complex, which, however, is somewhat unclear in this case).[51]

Acknowledgment. In memory of Swiatoslaw (Jerry) Trofimenko, the pioneer of scorpionate ligands. This work was supported by the Grant-in-Aid for Scientific Research (B) (No. 17350043) from the Japan Society of the Promotion of Science (to K.F.) and the Fonds der Chemischen Industrie (FCI) (to F.P. and N.L.).

Supporting Information Available: Complete ref 39, crystallographic data (Table S1), complete atomic labels (Figures S1 and S2), vibrational (IR) and electronic absorption spectra for **1** and **2** (Figures S3−S7, S9), [Cu(L3)] skeletal mode (Figure S8), table of DFT geometry optimized structures and vibrational frequencies for models of **1** and **2** using different combinations of functionals and basis sets (see Experimental Section) (Table S2), table of the results of TD-DFT calculations for **1** (Table S3). This material is available free of charge via the Internet at http://pubs.acs.org.

JA075071D

(51) Wilmot, C. M.; Hajdu, J.; McPherson, M. J.; Knowles, P. F.; Phillips, S. E. V. *Science* **1999**, *286*, 1724−1728.
(52) Fadini, A.; Schnepel, F.-M. *Schwingungsspektroskopie*; Thieme Verlag: Stuttgart, 1985.